INTERNATIONAL JOURNAL FOR NUMERICAL METHODS IN FLUIDS, VOL. 14, 267–288 (1992)

SIMULATION OF SUPERSONIC AND HYPERSONIC FLOWS

J. F. MILTHORPE

Department of Mechanical Engineering, University College, University of New South Wales, Australian Defence Force Academy, Campbell, ACT 2600, Australia

SUMMARY

A simple convection algorithm for simulation of time-dependent supersonic and hypersonic flows of a perfect but viscous gas is described. The algorithm is based on conservation and convection of mass, momentum and energy in a grid of rectangular cells. Examples are given for starting flow in a shock tube and oblique shocks generated by a wedge at Mach numbers up to 30·4. Good comparisons are achieved with well-known perfect gas flows.

KEY WORDS Compressible flow Hypersonic Perfect gas Time-dependent Convection method

INTRODUCTION

The prediction of supersonic and hypersonic flows continues to be a significant problem in fluid mechanics despite a great deal of work over many years. Some recent contributions have been made by, for example, Boris and Book,[1] Löhner *et al.*,[2] Chakravarthy and Osher,[3] Yee *et al.*[4] and Schmidt and Jameson.[5]

The existing computation methods for the supersonic flow problem are typically based on continuum mechanics. In this approach the problem of predicting the flow is regarded as a problem of solving partial differential equations subject to certain boundary conditions. These equations are then approximated by a numerical scheme which is based on Taylor series expansion of the governing differential equations.

These schemes assumes that the variables of the problem — velocity, pressure, temperature or some constructs of these — are continuous functions of space and time. The weakness of schemes based on the continuity assumption is naturally most clearly seen at shocks. Shocks are on the one hand the most characteristic feature of supersonic flow and on the other hand clear violations of the assumption of continuity.

The most superficial acquaintance with Fourier analysis indicates the way in which a set of continuous functions will represent a discontinuity: by a series of wiggles around the discontinuity which decrease in amplitude with distance from the shock. The typical shock prediction demonstrates this behaviour perfectly. The more advanced algorithms include correction to suppress this behaviour.

The traditional alternative method for the prediction of supersonic flows is the method of characteristics. On the basis of the hyperbolic nature of the governing equations, this method converts the partial differential equation problem into the solution of ordinary differential equations along characteristic lines. The disadvantage of this method is the complexity of the

0271–2091/92/030267–22$11.00

Received August 1990
Revised April 1991

process of evaluating the location of solution points from the intersection of the characteristic lines. A variant of the method of characteristics employs a fixed grid and assumes that the characteristics are piecewise straight. As a consequence the shocks are inaccurately located.

The error made by the classical type of algorithm is the assumption of continuity in discontinuous functions. The scheme advanced in this paper makes the opposite error: the solution functions are assumed to be discontinuous but the discontinuities are located in the wrong places.

The method does not attempt to solve the partial differential equations but rather examines the behaviour of the fundamental quantities: material, momentum and energy. As mentioned above, the governing equations of supersonic flow are hyperbolic in nature. Information propagates within a cone defined by the characteristics. In consequence the flow is controlled by the conditions upstream. It might appear that the downstream conditions have no effect on the flow, but this is not the case. A powerful early demonstration of this point was given by Roache.[6]

TYPICAL SUPERSONIC FLOW PROBLEMS

The flow problems described in this paper are typical of those in the literature. We can divide these into two classes: those with a defined flow rate and those in which the flow rate is determined in the calculation. We will describe the implementation of the boundary conditions for both classes and will deal first with those problems with a defined flow rate. A sample geometry, which exhibits most of the types of boundary condition in a fairly general form, is given in Figure 1 for flow over a wedge of half-angle 18·4°.

The fluid enters the computational domain at the upstream surface A with given properties: velocity, density, pressure, temperature and so on. This type of boundary condition presents no computational difficulties whatsoever: the values are simply specified.

A feature which often appears is a symmetry surface or slip plane (B in Figure 1). There is no flow across this surface, no shear stress and no diffusion of energy or material. These conditions occur at a plane of symmetry, on the centreline of an axisymmetric flow and at a solid surface at which it is not required to enforce a no-slip condition. These conditions are achieved in this

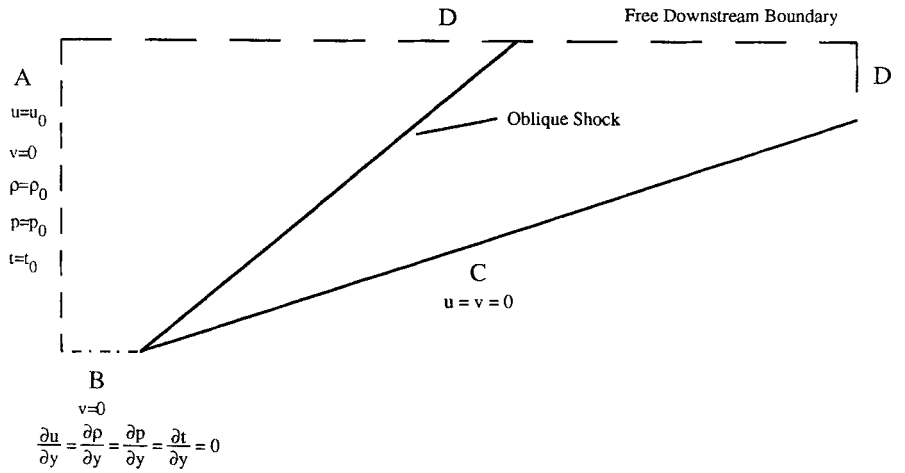

Figure 1. Example problem geometry for supersonic flow over wedge with half-angle 18·4°. The upstream flow conditions are fully specified and the downstream boundary condition is as described in the text

method by setting the values of all variables in the dummy layer immediately outside the computation domain to equal those inside, ensuring no diffusion across the boundary. The only restriction on the values in the surface layer is that the normal velocity is required to be not into the boundary. The values in any cell are of course only a representative average of the point values, so non-zero velocities into the computational domain do not violate the condition of zero flow through the boundary. Since the velocity in the surface layer is required to be zero or into the domain, there can be no flow outwards across the boundary. The normal velocity in the dummy layer is set to zero and hence there is no flow inwards across the boundary.

It is not possible to set the normal velocity in the surface layer to zero, since it would then be impossible for material to leave the cells in the surface layer. A zero tangential velocity is required at some point in the surface layer where an object is placed in the flow. For the class of problems we are discussing in this section the upstream conditions include a defined velocity and so the quantity of material in the surface layer cells would grow continuously with time.

FREE DOWNSTREAM BOUNDARY CONDITIONS

The free downstream boundary condition, D in Figure 1, is by far the most difficult to implement successfully. In contrast to the predetermined downstream condition, such as a set value of pressure in the free stream, no information is known about the conditions at a free downstream boundary, except that no influence from the boundary can be allowed to propagate into the flow upstream.

Although difficult, the free downstream boundary condition is a very important one both for practical computation and for verification of the algorithm. The simple analytical results in compressible flow are obtained for perfect gases, and if a number of shocks occur in the flow, the influence of the steadily growing boundary layer will make the expected real results differ greatly from the perfect gas theory; but it is not possible to calculate exactly the real flow, except by the use of the kind of algorithm we are testing. A simple flow, such as the oblique shock wave produced by a wedge, will not differ greatly from the corresponding perfect gas flow, and the difference can be reasonably estimated. It is therefore desirable for verification to be able to simulate the flow past a wedge in an infinite gas. For a computer of finite size this requires a free boundary. Many, perhaps most, experimental results are concerned with external flows and these similarly require free downstream boundaries if the size of the computation domain is to be at all reasonable.

A similar type of condition is sometimes applied in incompressible flow if a stress-free downstream boundary is imposed, but this does not lead to the difficulties encountered in compressible flow. These difficulties were first reported by Roache.[6] Complete specification of the upstream values should determine flow everywhere, provided that the flow remains supersonic. The algorithm described here resembles almost all others in possessing a small amount of 'numerical viscosity': diffusion of various quantities in all directions, including upsteam. In consequence it is necessary to supply the correct values on the downstream boundary so as not to impose a false resistance to the flow: the author has found it possible to impose either a resistance or apply an acceleration to the flow if incorrect values are applied at the downstream boundary.

The downstream condition which has proved successful with the algorithm described attempts to estimate the flow conditions outside the boundary from those just inside the boundary. Two alternative conditions were tried. The first was to calculate the values outside the boundary from those directly upstream. In the second the values are projected along the characteristic direcions. The first condition produced a false acceleration in the flow in the region where the shock

intersects the boundary. The second condition produced a resistance to flow in the same region and created a weak reflected shock.

The condition adopted is to project the contours of the flow variables across the boundary. The direction of the contours at the boundary is determined for each cell by calculating the direction which gives the minimum average deviation from the contour value. The value outside the boundary is taken as the mean value along that direction for a small distance into the region. The distance is typically 10 cells. It will be seen from the results shown below that this condition gives quite straight projection of the contours over the boundary.

CONSERVATION ALGORITHM

The algorithm used to calculate the flow values is based on conservation of mass, momentum and energy as the simulation proceeds over discrete time steps. The flow domain is divided into rectangular cells. Each cell contains at any given time a certain block of material which possesses a certain momentum and energy. In the course of the next time step this block, with its associated mass, momentum and energy, is convected a small distance. It may also gain or lose mass, momentum or energy by diffusion and the action of pressure gradients. The algorithm evaluates the changes in these quantities for the material block and proportionally redistributes the mass, momentum and energy to the cells over which the block is located at the end of the time step.

The mechanism of the algorithm is illustrated in Figure 2 for convection with positive u- and v-velocities. The letters A, B, C and D represent the proportion of the material block located in a particular cell at the end of a time step. These proportions of mass, momentum and energy in the material block are allocated to their respective cells. When the process has been performed for all cells, the new distribution of mass, momentum and energy is available. From this distribution updated values of density, velocity, pressure and temperature can be derived. Upwinding is used in the evaluation of the momentum and energy changes produced by the pressure gradients in order to prevent instabilities.

The flow quantities are transported by three processes modelled by the algorithm. Least significant in magnitude is diffusive transport of mass, momentum and energy. Secondly, there is the mechanical transport of momentum and energy due to pressure differences between the cells. Greatest in magnitude at the velocities modelled is convective transport of mass, momentum and energy due to the velocity of the fluid relative to the mesh of cells.

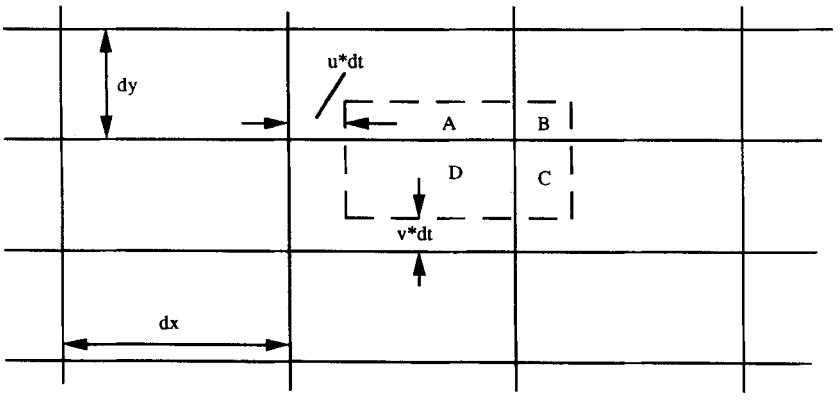

Figure 2. Convection of material block with velocity u, v during one time step dt. See text for description of convection algorithm

Calculation of the flow quantities at the next time step is done in the following sequence. The mass, momentum and energy in a cell are modified by the action of diffusion:

$$dQ^k_{i,j}=\delta t\alpha^k[dy(Q^k_{i-1,j}-2Q^k_{i,j}+Q^k_{i+1,j})+dx(Q^k_{i,j-1}-2Q^k_{i,j}+Q^k_{i,j+1})], \quad (1)$$

where $Q^k_{i,j}$ is the quantity of mass, momentum or energy in the (i,j)th cell and α^k is the corresponding diffusion coefficient. The cell sides have dimensions dx and dy and the time step is δt. In addition, momentum and energy are modified by diffusion of those quantities along velocity gradients and energy is modified by diffusion along temperature gradients, which are calculated in the same way.

In the second phase of transport calculation the momentum and energy in the cell are modified by the action of the pressure gradients. The pressure difference between adjacent cells moves momentum between the cells in accord with the relations

$$\delta(\rho u_{i,j})=\delta t\, dy(p_{i-1,j}-2p_{i,j}+p_{i+1,j}),$$

$$\delta(\rho v_{i,j})=\delta t\, dx(p_{i,j-1}-2p_{i,j}+p_{i,j+1}),$$

where $\delta(\rho u_{i,j})$ and $\delta(\rho v_{i,j})$ are the changes in x- and y-momentum at the (i,j)th cell. In the implementation of the algorithm it has been necessary to use local upwinding in the evaluation of the momentum transport due to pressure gradients. The upwinding velocity at a cell is taken as the average velocity over a group of 24 surrounding cells. The x-momentum transported into the (i,j)th cell is calculated as

$$\delta(\rho u)=\delta t\, dy\tfrac{1}{2}[(1+F)p_{i-1,j}+2Fp_{i,j}-(1-F)p_{i+1,j}], \quad (2)$$

where F is the upwinding factor, such that $F=1$ gives complete upwinding with a positive u-velocity. The y-momentum transport is calculated in the same way. The value chosen for the upwinding factor in applications of this algorithm is $F=\pm 0{\cdot}9$ depending on the sign of the local average u-velocity. This value has been selected after a very limited amount of experiment. Development work is required to determine the best value for the upwinding factor.

At the same time as the pressure gradients are transporting momentum between adjacent cells, they are also doing work, if the local velocity is non-zero, and hence transporting energy between the cells. This energy transport is obtained from the momentum transport calculated at (2) by multiplying by the local velocity.

The third phase of mass, momentum and energy transport algorithm is the convection of the cells. This is illustrated in Figure 2 for convection with positive u- and v-velocities. A cell is regarded as moving with unchanged dimensions relative to the mesh of cell boundaries, so that it overlaps adjacent cells. The letter A indicates the area of the cell which remains in the original cell at the end of the time step, while B, C and D represent the areas of a cell which are located in adjacent cells. The quantities of mass, momentum and energy in the cell are divided in proportion to the areas A, B, C and D. Those proportions represented by B, C and D are subtracted from the quantities in the original cell and added to the appropriate adjacent cells.

When the adjustment of mass, momentum and energy has been completed for all cells, the flow variables ρ, u, v, p and t can be calculated for all cells.

The algorithm requires approximately 0·05 s of CPU time on a PRIME 9955 minicomputer to update one cell for one time step.

STABILITY LIMITS

It is more economical to use the largest possible time step in the computations, but there are a number of limits imposed by accuracy and stability considerations. The first is that, since

convection is only calculated into the adjacent cells, the distance travelled in a time step must not exceed the cell dimension. The second limit is that due to overprediction of diffusion, as described by Roache,[6] which restricts the time step to

$$\Delta t < \rho \Delta x^2 / 2k, \tag{3}$$

where Δx is the step size, ρ is the density and k is the diffusion coefficient for any quantity.

TRANSIENT NORMAL SHOCK

The algorithm has been tested with a number of flows involving unsteady normal shocks at a range of Mach numbers. The flow conditions were deliberately selected to give a mismatch between upstream and downstream values, and the typical flow geometry is shown in Figure 3. Since the density ratio across the shock system exceeds the limiting value, equal to 6 for air, the compression takes place in two stages. There is no limit on the density rise across the contact surface, since no gas flow occurs. The intermediate pressure p_2, referring to the regions 1–4 shown in Figure 3, is given by[7]

$$\frac{p_4}{p_1} = \frac{p_2}{p_1}\left(1 - \frac{(\gamma_4 - 1)(a_1/a_4)(p_2/p_1 - 1)}{\sqrt{(2\gamma_1)}\sqrt{[2\gamma_1 + (\gamma_1 - 1)(p_2/p_1 - 1)]}}\right)^{-1/\nu}. \tag{4}$$

The other intermediate values follow from the pressure by the standard perfect gas equations.[8] It can be seen from Figure 3 that although the flow is one-dimensional, the algorithm is applied to a two-dimensional domain with a symmetry plane on the lower surface and a free downstream boundary on the upper surface. These conditions were selected to provide a thorough test for the algorithm.

The results obtained for a range of Mach numbers are shown in Figures 4–9. In each figure the perfect gas solution at the simulated time is superimposed on the calculated result. The grid used in the computations was 498 cells long by 28 cells wide and the cells were squares of side 0·5. The

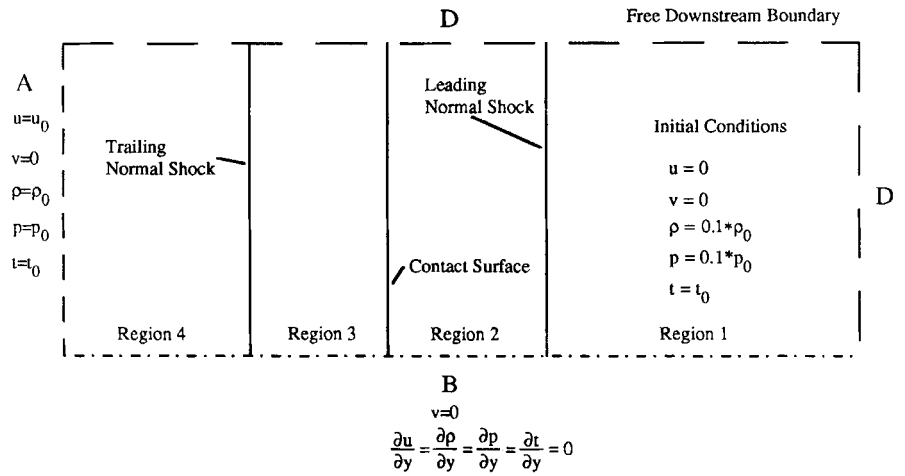

Figure 3. Example flow geometry for supersonic flow with mismatched upstream and initial conditions. The upstream and initial flow conditions are fully specified and the downstream boundary conditions are as described in the text

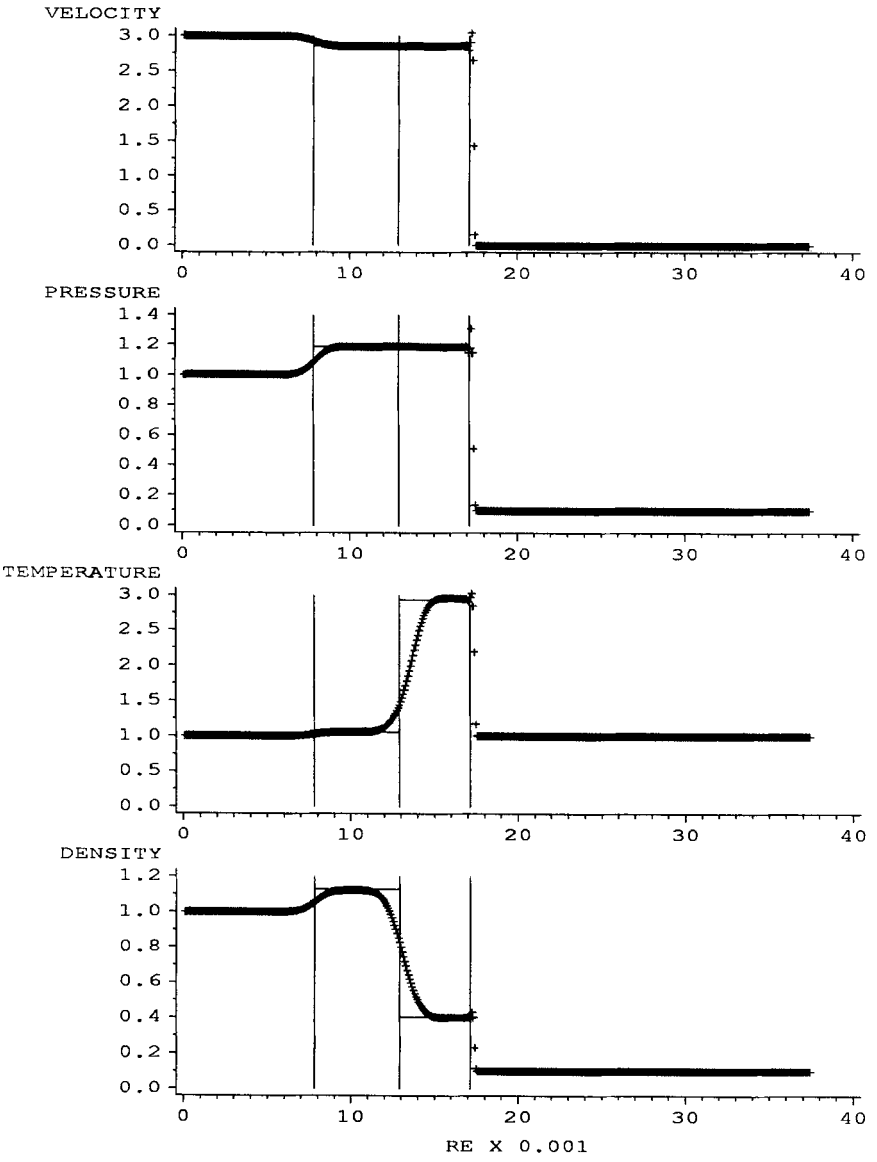

Figure 4. Mismatched normal shocks moving into quiescent gas with inlet Mach number 2·54 at non-dimensional time 5324 (see text). Pressure and density ratios are 10. The resultant incident shock Mach number is 3·208. The thin vertical lines indicate the position of the invisicid normal shocks and contact surface and the thin horizontal lines the value of the invisicid solution between the shocks at the same time

abscissa in the figures has a scale of Reynolds numbers

$$Re = \rho_0 u_0 x / v, \tag{5}$$

where ρ_0 is the inlet density, u_0 is the inlet velocity, v is the viscosity of the gas and x is the distance from the inlet boundary.

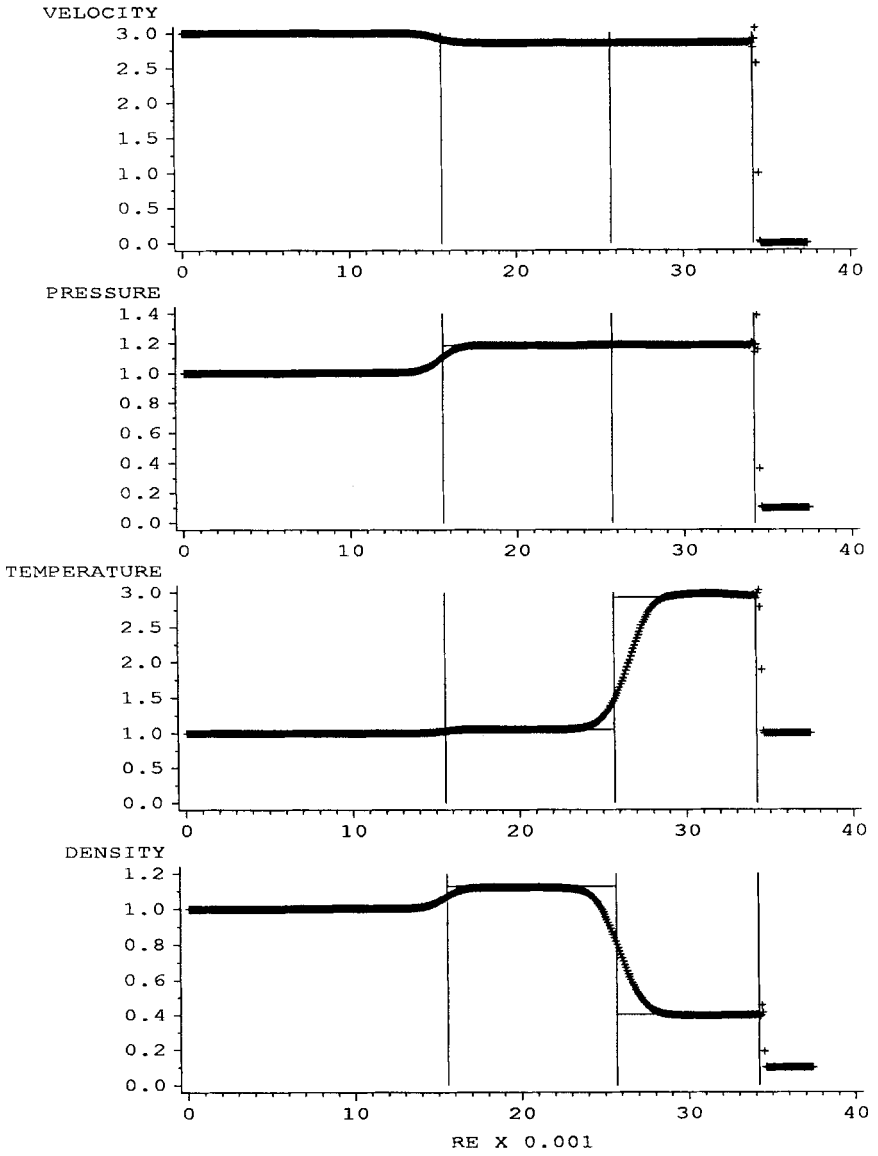

Figure 5. Mismatched normal shocks moving into quiescent gas with inlet Mach number 2·54 at non-dimensional time 10 649 (see text). Pressure and density ratios are 10. The resultant incident shock Mach number is 3·208. The thin vertical lines indicate the position of the invisicid normal shocks and contact surface and the thin horizontal lines the value of the invisicid solution between the shocks at the same time

It should be noted that the viscosity is constant in all the examples given in this paper: no attempt is made to account for variation with temperature. It is intended to introduce these and other real gas effects in later work.

The non-dimensional time t_{nd} shown is given by

$$t_{nd} = t_{model}(\rho_0 u_0 a_0 / \nu), \tag{6}$$

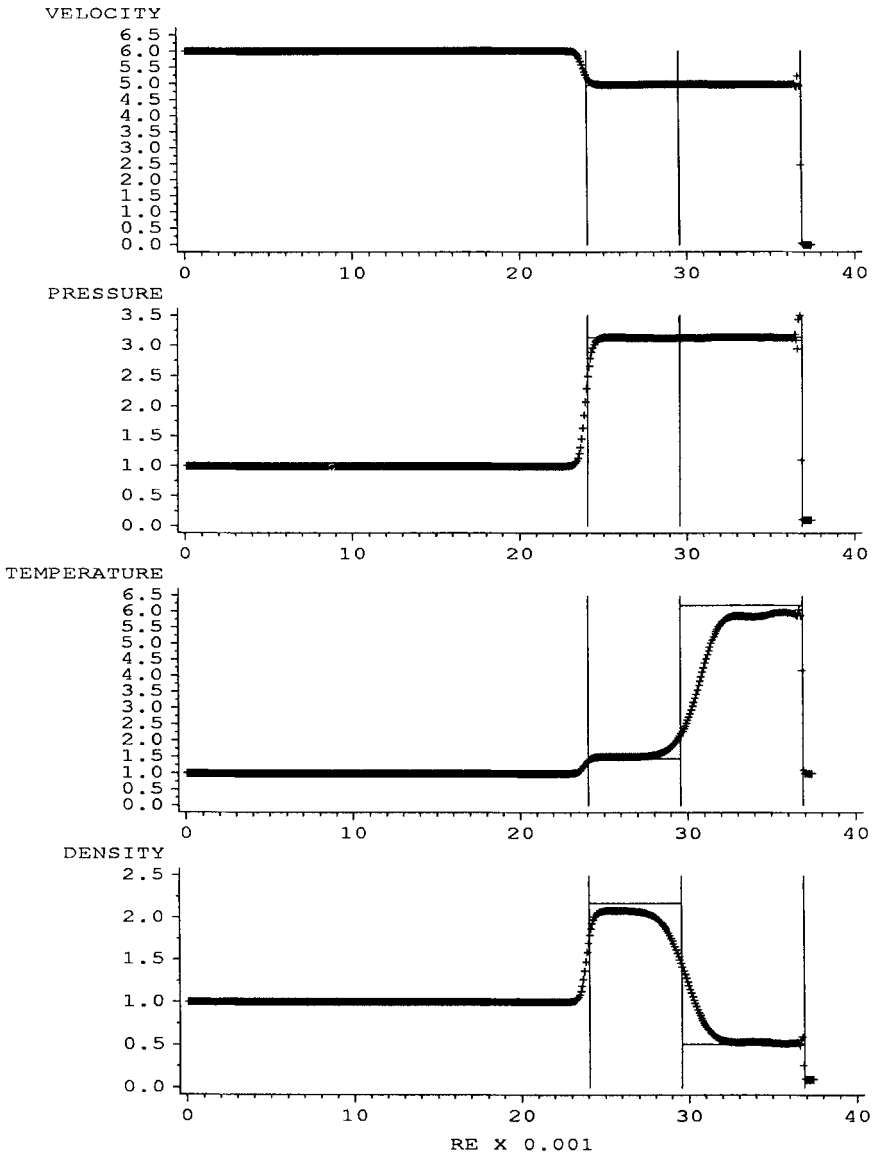

Figure 6. Mismatched normal shocks moving into quiescent gas with inlet Mach number 5·07 at non-dimensional time 7099 (see text). Pressure and density ratios are 10. The resultant incident shock Mach number is 5·192. The thin vertical lines indicate the position of the invisicid normal shocks and contact surface and the thin horizontal lines the value of the invisicid solution between the shocks at the same time

where t_{model} is the time in model units and a_0 is the inlet speed of sound. The wide variation in Reynolds number scales and non-dimensional times is due to the range of viscosities employed, which varies from 0·04 to 0·15.

The leading shock is sharply defined in all cases, while the contact surface and trailing shock are smeared out to some extent. It was not at first clear whether the smearing was caused by the

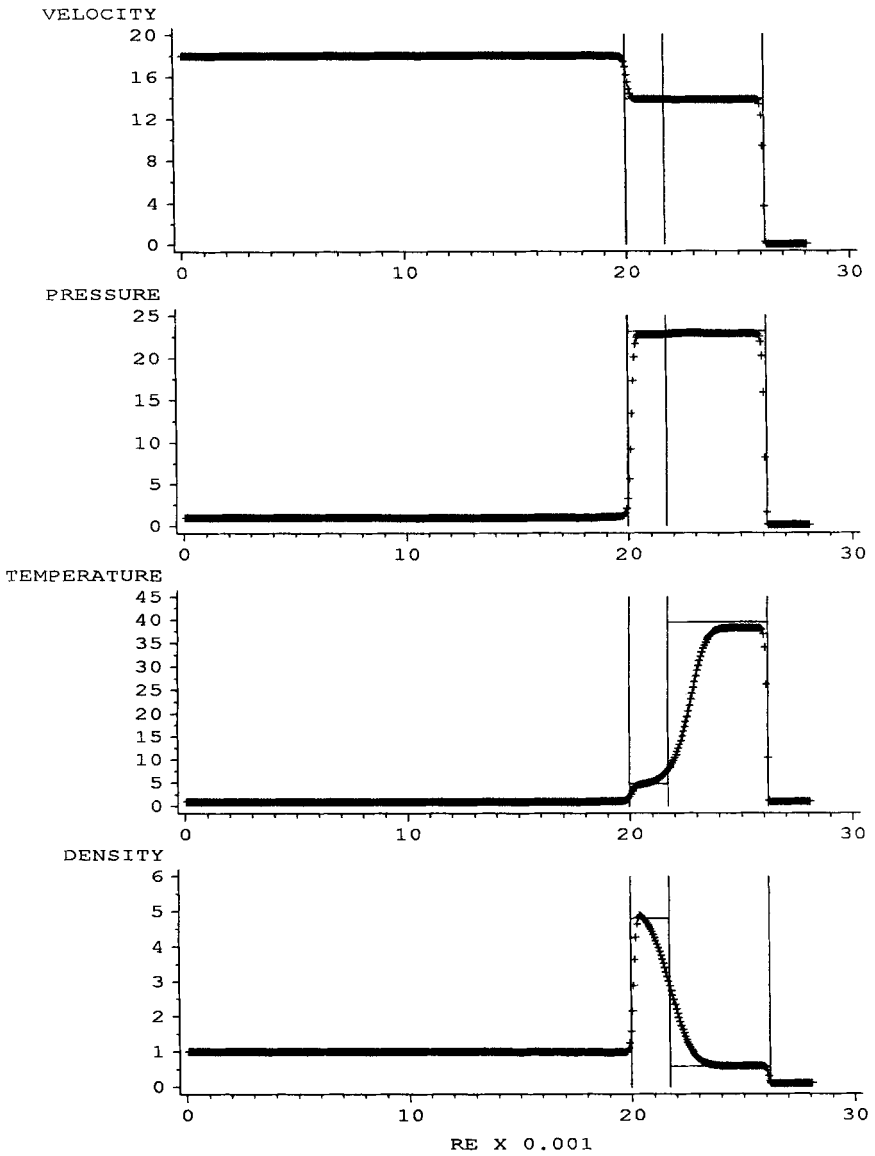

Figure 7. Mismatched normal shocks moving into quiescent gas with inlet Mach number 15·2 at non-dimensional time 1988 (see text). Pressure and density ratios are 10. The resultant incident shock Mach number is 16·66. The thin vertical lines indicate the position of the invisicid normal shocks and contact surface and the thin horizontal lines the value of the invisicid solution between the shocks at the same time

algorithm or by the starting process: at time zero the shocks and contact surface are co-located at $Re=0$. The result shown in Figure 7 is for a flow which was started with the sharply defined perfect gas solution fully represented in the flow: it can be seen that smearing is very similar to that in a flow which has been through the complex starting flow. The smearing is a product of the

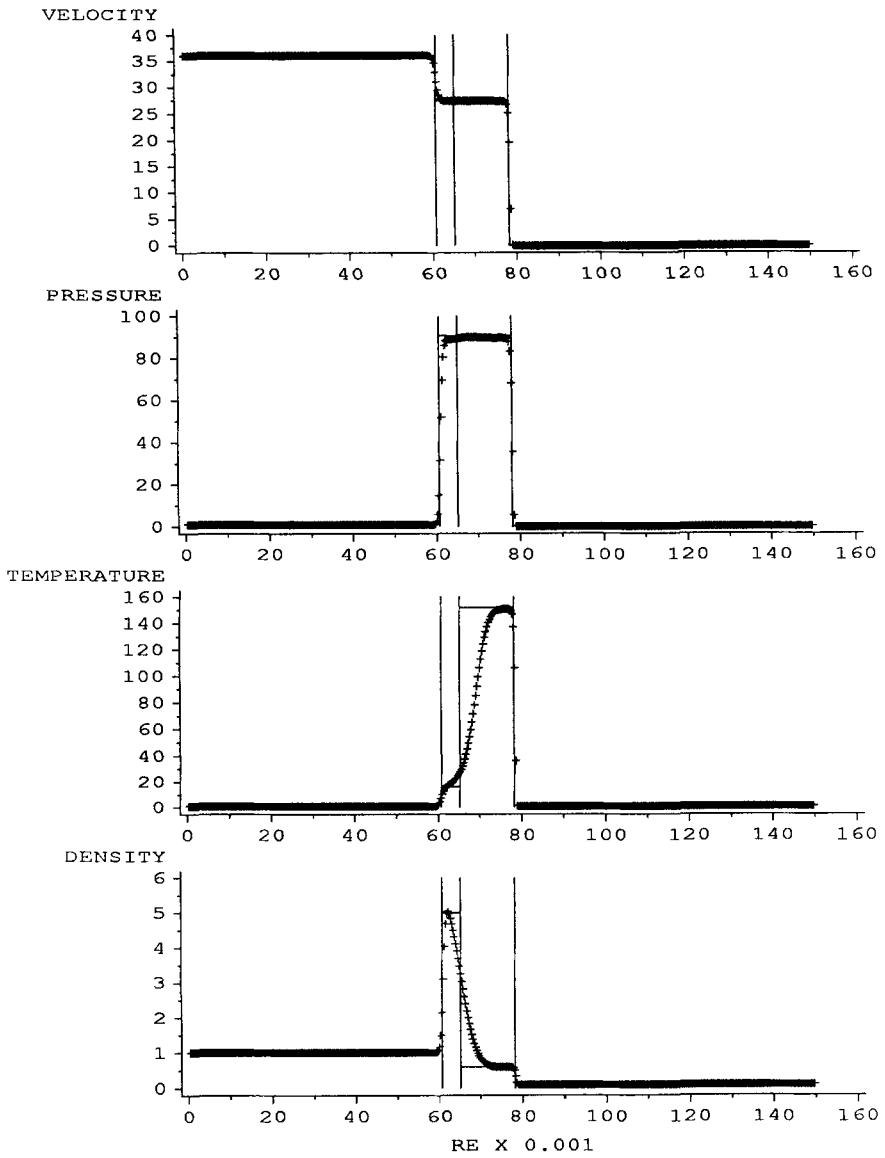

Figure 8. Mismatched normal shocks moving into quiescent gas with inlet Mach number 30·4 at non-dimensional time 4970 (see text). Pressure and density ratios are 10. The resultant incident shock Mach number is 32·95. The thin vertical lines indicate the position of the invisicid normal shocks and contact surface and the thin horizontal lines the value of the invisicid solution between the shocks at the same time

algorithm, though it is still not clear whether the effect is caused by the simulated viscosity or by numerical diffusion.

The results shown demonstrate that, apart from the smearing of the contact surface and trailing shock, the algorithm accurately models the perfect gas theory at Mach numbers up to at least 27. The algorithm has not been tested at higher Mach numbers.

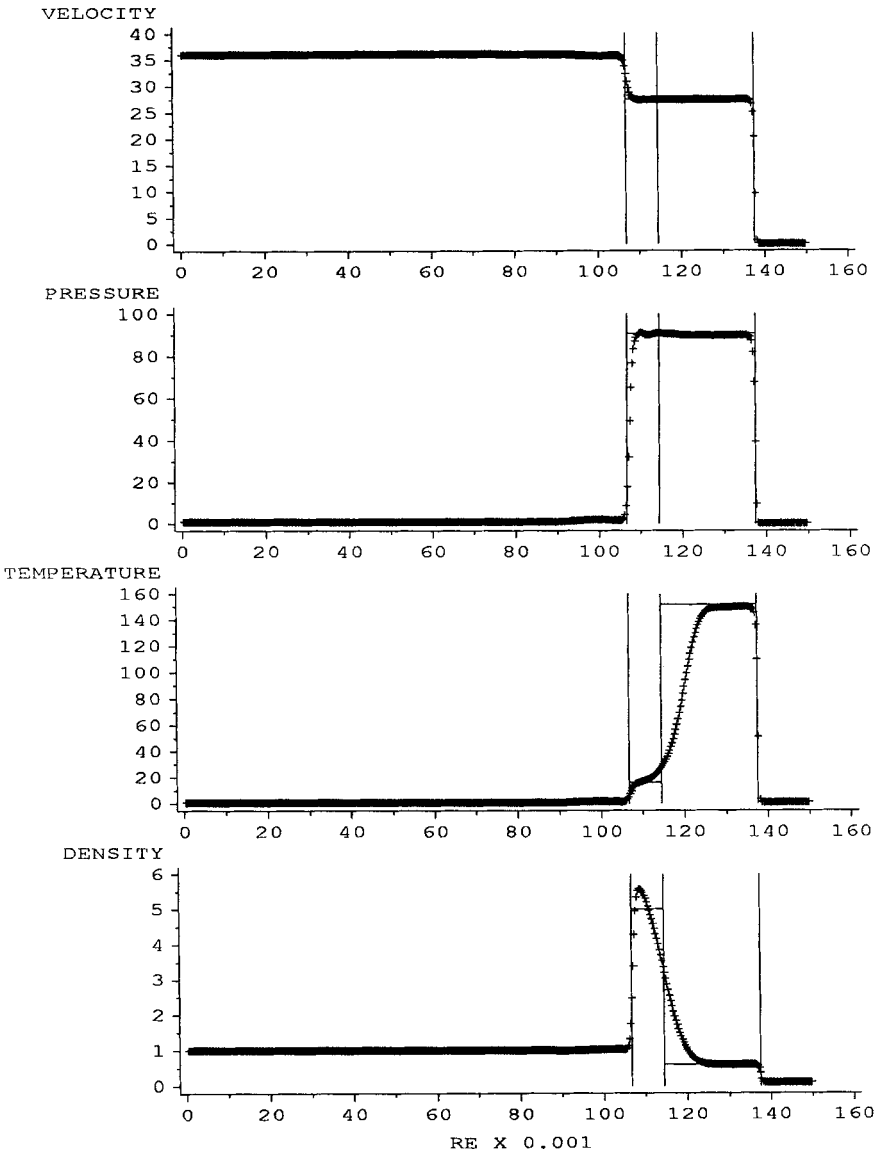

Figure 9. Mismatched normal shocks moving into quiescent gas with inlet Mach number 30·4 at non-dimensional time 7099 (see text). Pressure and density ratios are 10. The resultant incident shock Mach number is 32·95. The thin vertical lines indicate the position of the invisicid normal shocks and contact surface and the thin horizontal lines the value of the invisicid solution between the shocks at the same time

EXAMPLE PROBLEM

The problem shown in Figure 1 has been used as an example to test the effectiveness of the algorithm. The particular values used were

$$u_0 = 3{\cdot}0, \tag{7}$$

$$\rho_0 = p_0 = t_0 = 1{\cdot}0, \tag{8}$$

and the gas was taken as a quasi-perfect gas with

$$\gamma = 1{\cdot}4. \tag{9}$$

The viscosity was set at the lowest value which would give stable solutions.

The steady state upstream Mach number M_0 of the flow is thus 2·54. The deflection angle θ in inviscid flow would be 18·4°. The angle of the oblique shock, β, and the downstream pressure p_1, density ρ_1, temperature t_1 and Mach number M_1 are obtained from the expressions

$$\tan\theta = \frac{M_0^2 \sin 2\beta - 2\cot\beta}{M_0^2(\gamma + \cos 2\beta) + 2}, \tag{10}$$

$$\frac{p_1}{p_0} = \frac{2\gamma}{\gamma+1} M_0^2 \sin^2\beta - \frac{\gamma-1}{\gamma+1}, \tag{11}$$

$$\frac{\rho_1}{\rho_0} = \frac{(\gamma-1)M_0^2 \sin^2\beta + 2}{(\gamma+1)M_0^2 + \sin^2\beta}, \tag{12}$$

$$\frac{t_1}{t_0} = \left(\frac{\gamma-1}{\gamma+1}\right)^2 \frac{\{[2\gamma/(\gamma-1)]M_0^2 \sin^2\beta - 1\}[M_0^2 \sin^2\beta + 2/(\gamma-1)]}{M_0^2 \sin^2\beta}, \tag{13}$$

$$M_1^2 \sin^2(\beta-\theta) = \frac{1 + [(\gamma-1)/2]M_0^2 \sin^2\beta}{\gamma M_0^2 \sin^2\beta - (\gamma-1)/2}. \tag{14}$$

Predictions obtained with the algorithm for Mach number 2·54 are shown in Figures 10–24. Results are given at three times, while the flow is developing and when a steady state has been reached. Contours of Mach number, density, pressure, temperature and speed are shown.

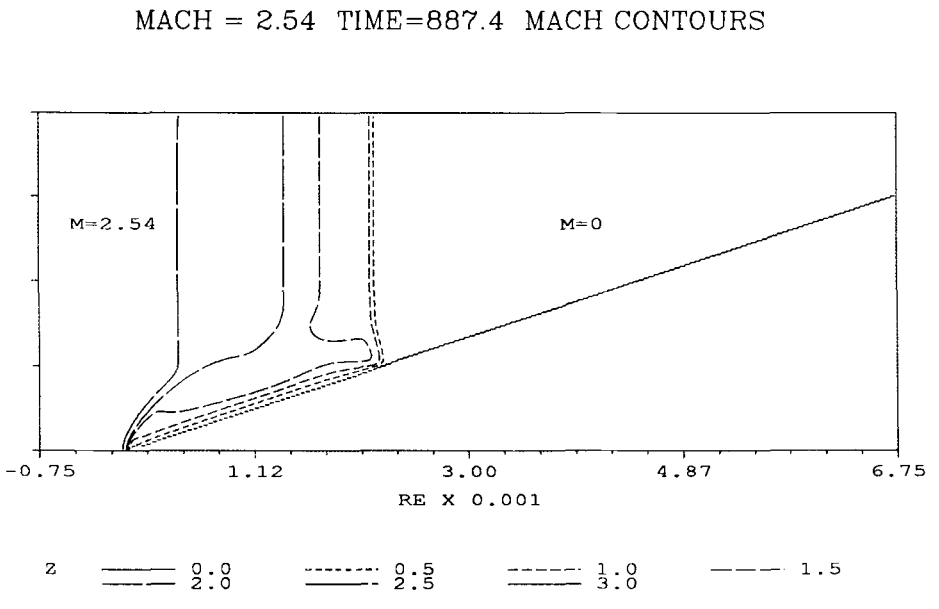

Figure 10. Mach number contours in transient flow over a wedge of half-angle 18·4° with incident Mach number 2·54. Mismatched normal shocks are moving into quiescent gas at non-dimensional time 887 (see text). Pressure and density ratios are 10

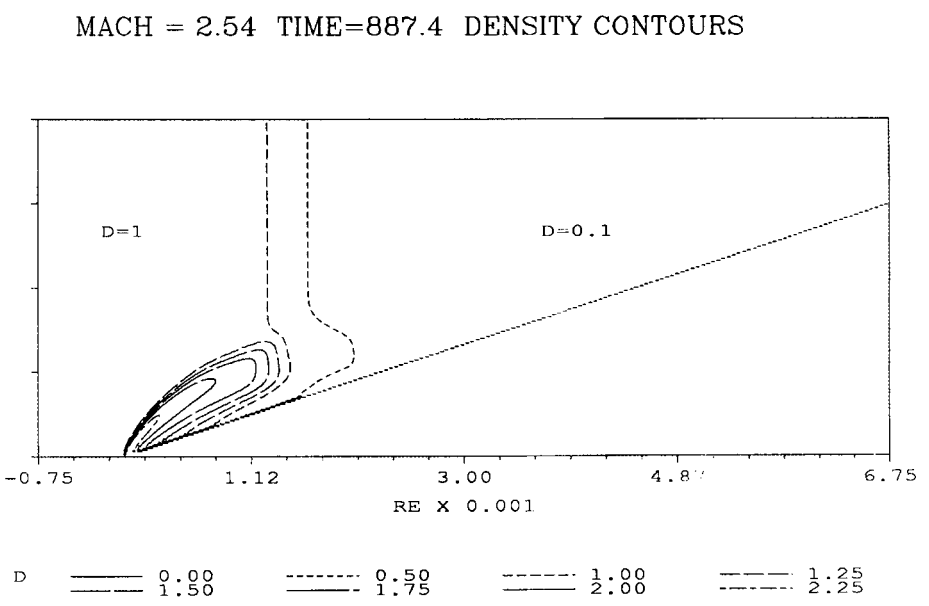

Figure 11. Density contours in transient flow over a wedge of half-angle 18·4° with incident Mach number 2·54. Mismatched normal shocks are moving into quiescent gas at non-dimensional time 887 (see text). Pressure and density ratios are 10

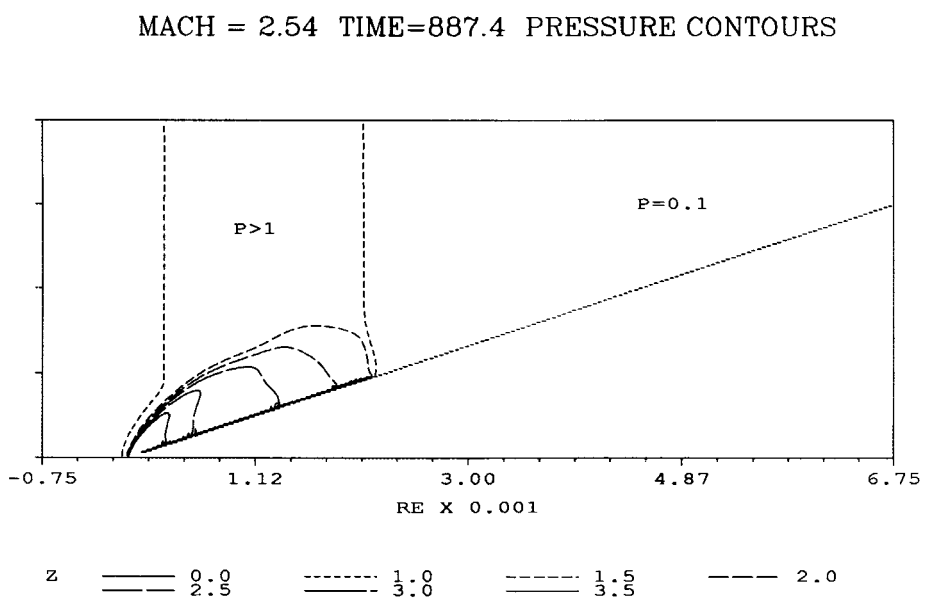

Figure 12. Pressure contours in transient flow over a wedge of half-angle 18·4° with incident Mach number 2·54. Mismatched normal shocks are moving into quiescent gas at non-dimensional time 887 (see text). Pressure and density ratios are 10

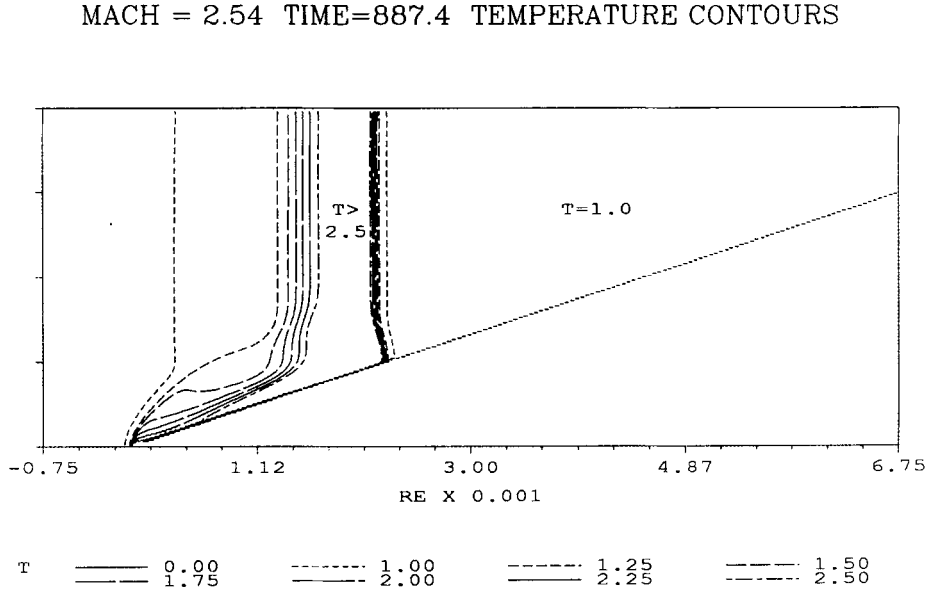

Figure 13. Temperature contours in transient flow over a wedge of half-angle 18·4° with incident Mach number 2·54. Mismatched normal shocks are moving into quiescent gas at non-dimensional time 887 (see text). Pressure and density ratios are 10

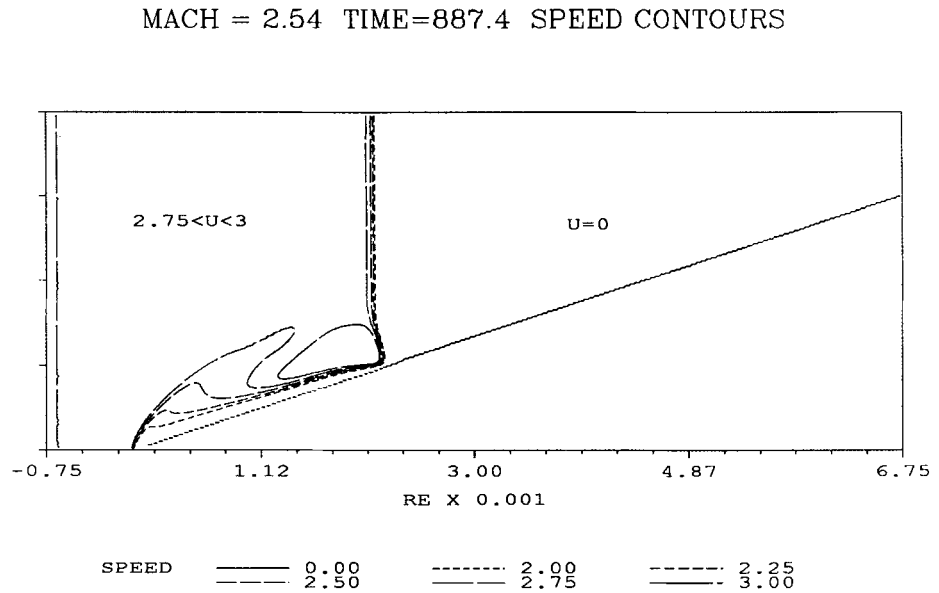

Figure 14. Speed contours in transient flow over a wedge of half-angle 18·4° with incident Mach number 2·54. Mismatched normal shocks are moving into quiescent gas at non-dimensional time 887 (see text). Pressure and density ratios are 10

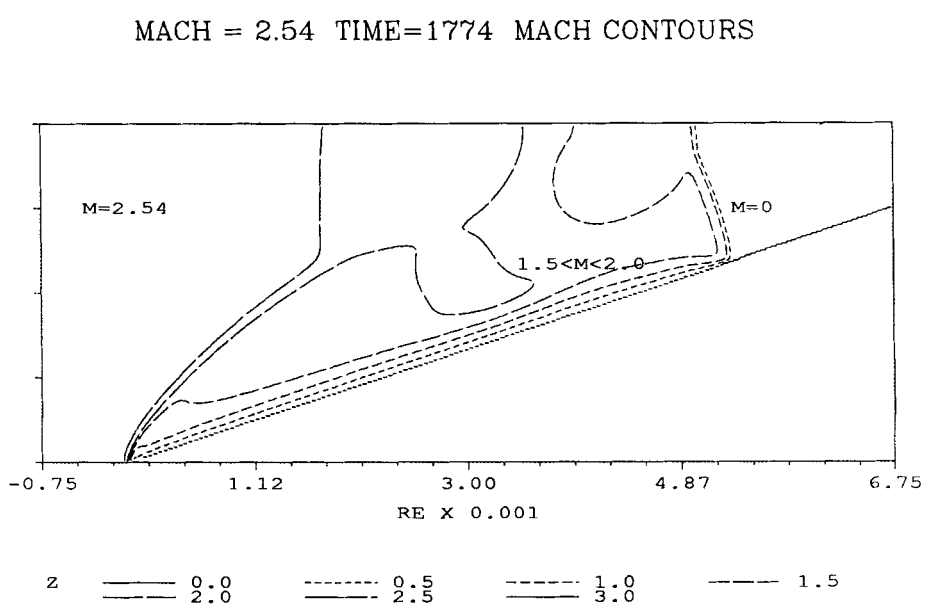

Figure 15. Mach number contours in transient flow over a wedge of half-angle 18·4° with incident Mach number 2·54. Mismatched normal shocks are moving into quiescent gas at non-dimensional time 1775 (see text). Pressure and density ratios are 10

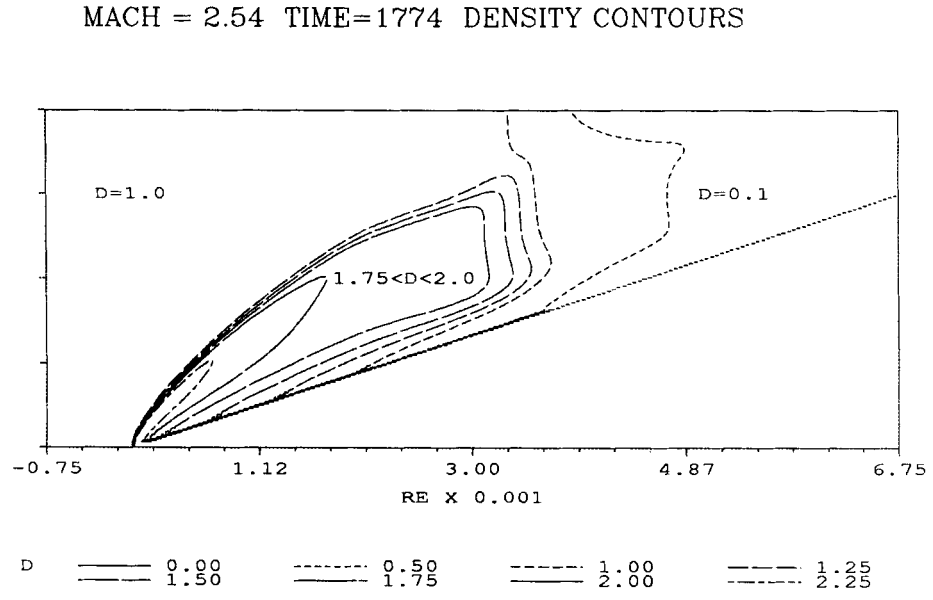

Figure 16. Density contours in transient flow over a wedge of half-angle 18·4° with incident Mach number 2·54. Mismatched normal shocks are moving into quiescent gas at non-dimensional time 1775 (see text). Pressure and density ratios are 10

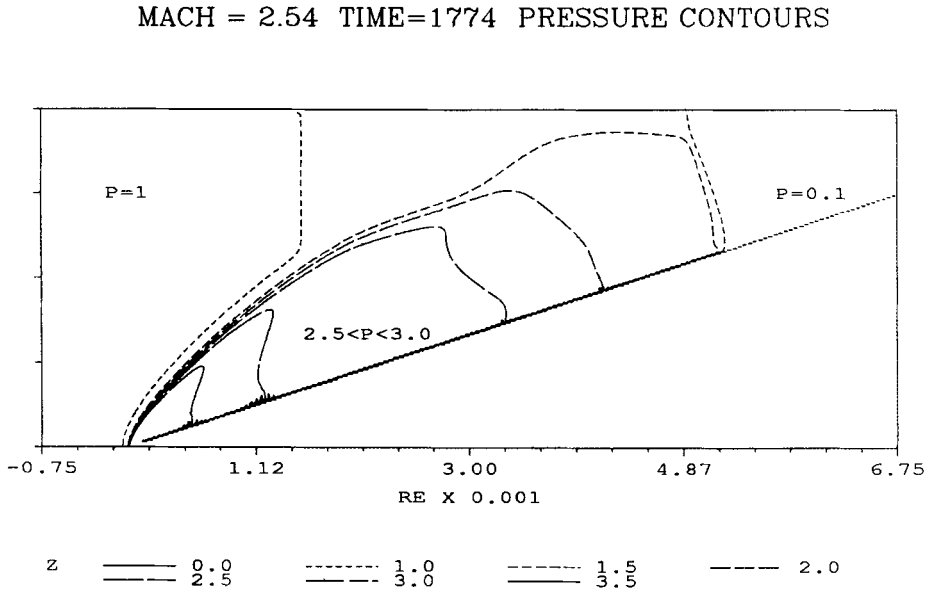

Figure 17. Pressure contours in transient flow over a wedge of half-angle 18·4° with incident Mach number 2·54. Mismatched normal shocks are moving into quiescent gas at non-dimensional time 1775 (see text). Pressure and density ratios are 10

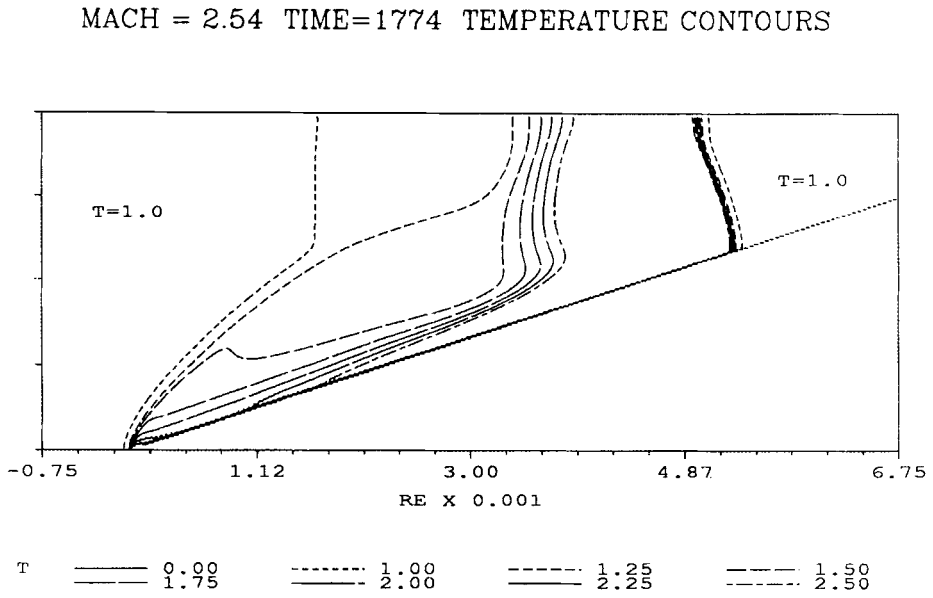

Figure 18. Temperature contours in transient flow over a wedge of half-angle 18·4° with incident Mach number 2·54. Mismatched normal shocks are moving into quiescent gas at non-dimensional time 1775 (see text). Pressure and density ratios are 10

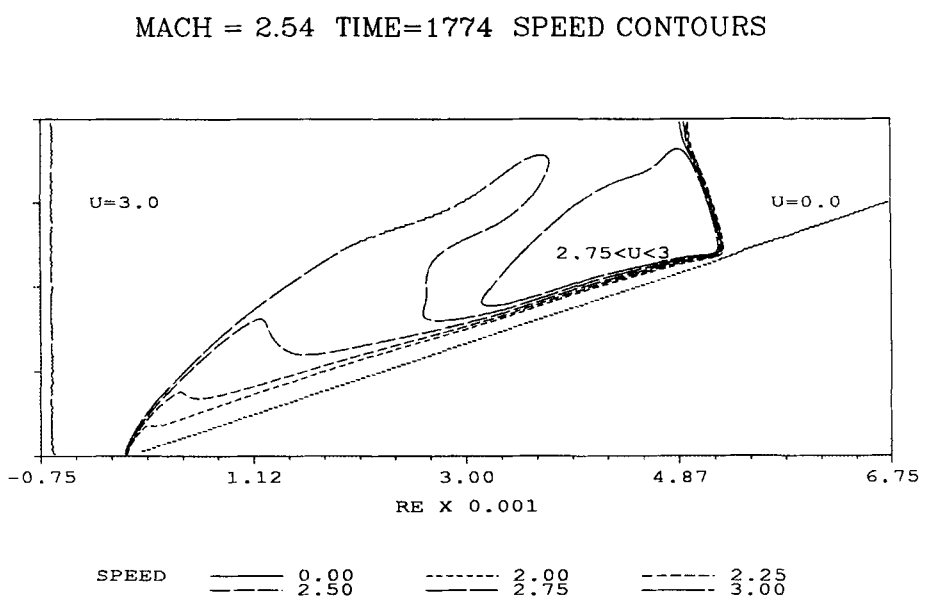

Figure 19. Speed contours in transient flow over a wedge of half-angle 18·4° with incident Mach number 2·54. Mismatched normal shocks are moving into quiescent gas at non-dimensional time 1775 (see text). Pressure and density ratios are 10

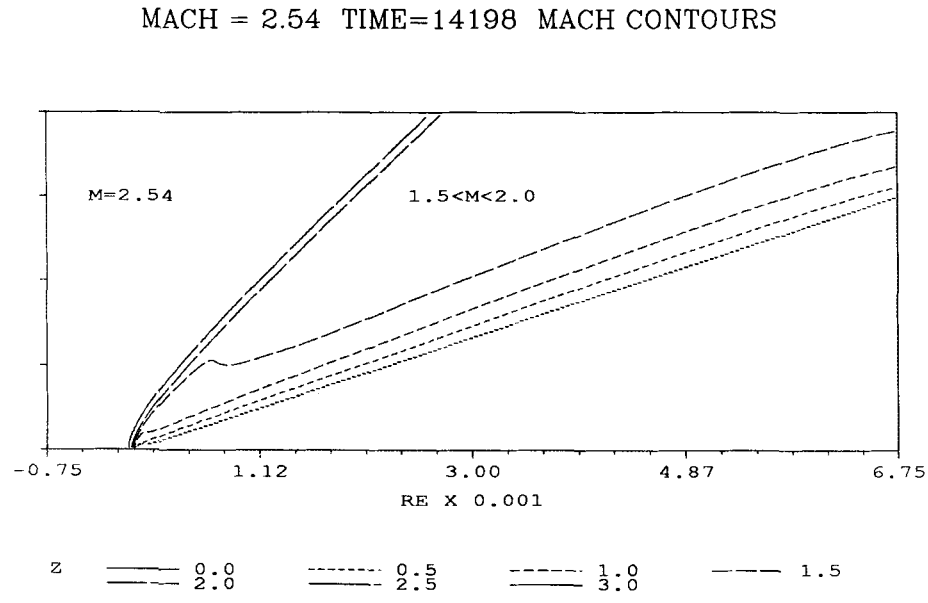

Figure 20. Mach number contours in steady state flow over a wedge of half-angle 18·4° with incident mach number 2·54. The non-dimensional time is 14198 (see text)

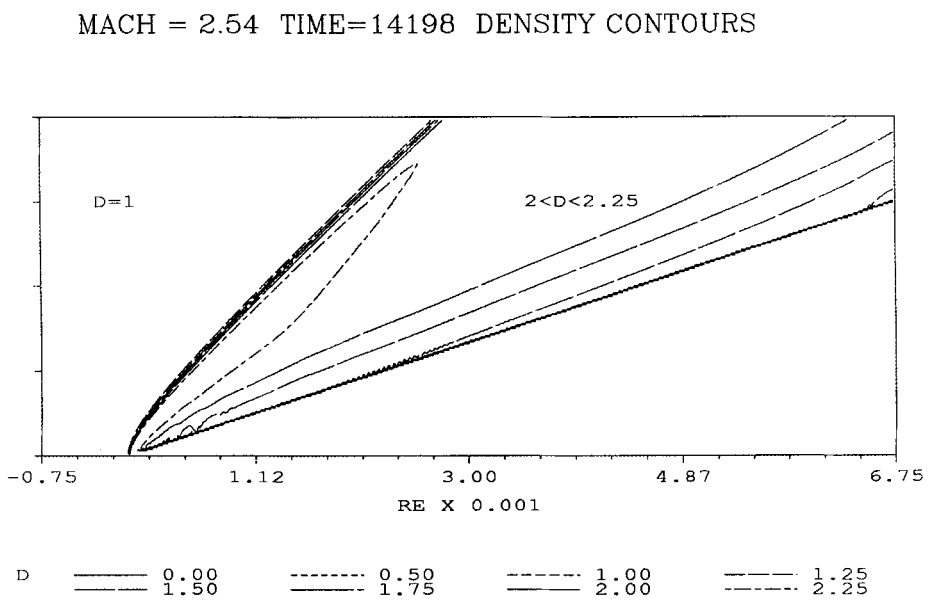

Figure 21. Density contours in steady state flow over a wedge of half-angle 18·4° with incident mach number 2·54. The non-dimensional time is 14198 (see text)

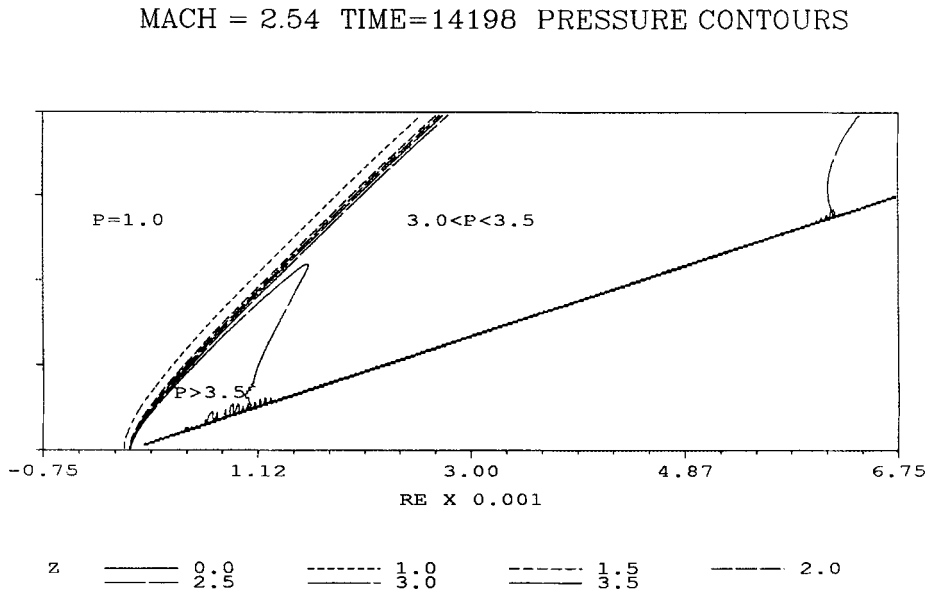

Figure 22. Pressure contours in steady state flow over a wedge of half-angle 18·4° with incident mach number 2·54. The non-dimensional time is 14198 (see text)

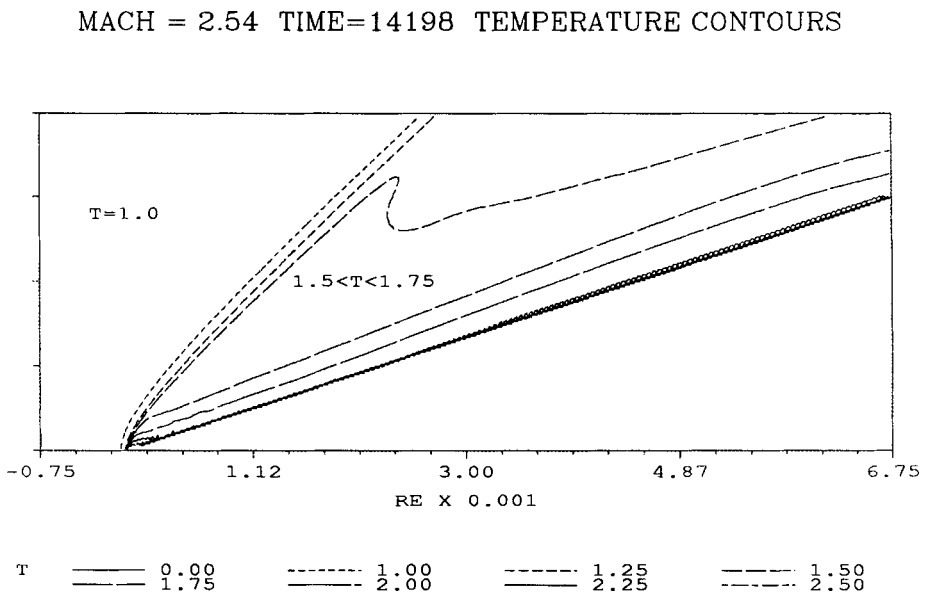

Figure 23. Temperature contours in steady state flow over a wedge of half-angle 18·4° with incident mach number 2·54. The non-dimensional time is 14198 (see text)

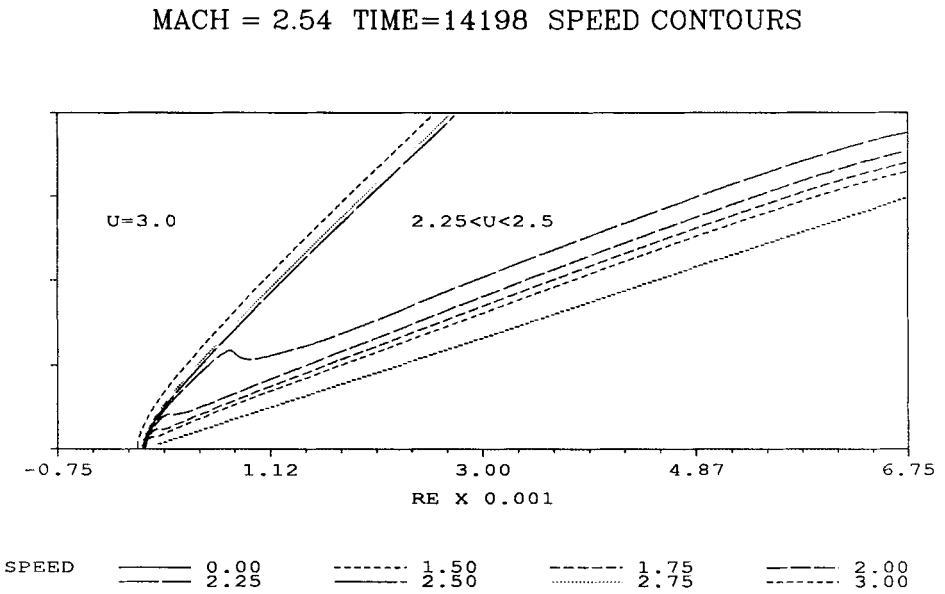

Figure 24. Speed contours in steady state flow over a wedge of half-angle 18·4° with incident mach number 2·54. The non-dimensional time is 14198 (see text)

The results are very similar to the inviscid predictions, except for the presence of the boundary layer. There is a small curved detached shock at the apex of the wedge and the oblique shock is at a slightly smaller angle. In Figures 10–19 the Mach stem at the base of the incident shock is clearly visible.

The presence of the boundary layer results in a deflection angle slightly larger than that due to the wedge alone, and hence the flow variables after the shock do not have the inviscid values. A test of the accuracy of the algorithm is to examine the change in flow variables normal to the oblique shock and compare these with the corresponding inviscid solution. This has been done in

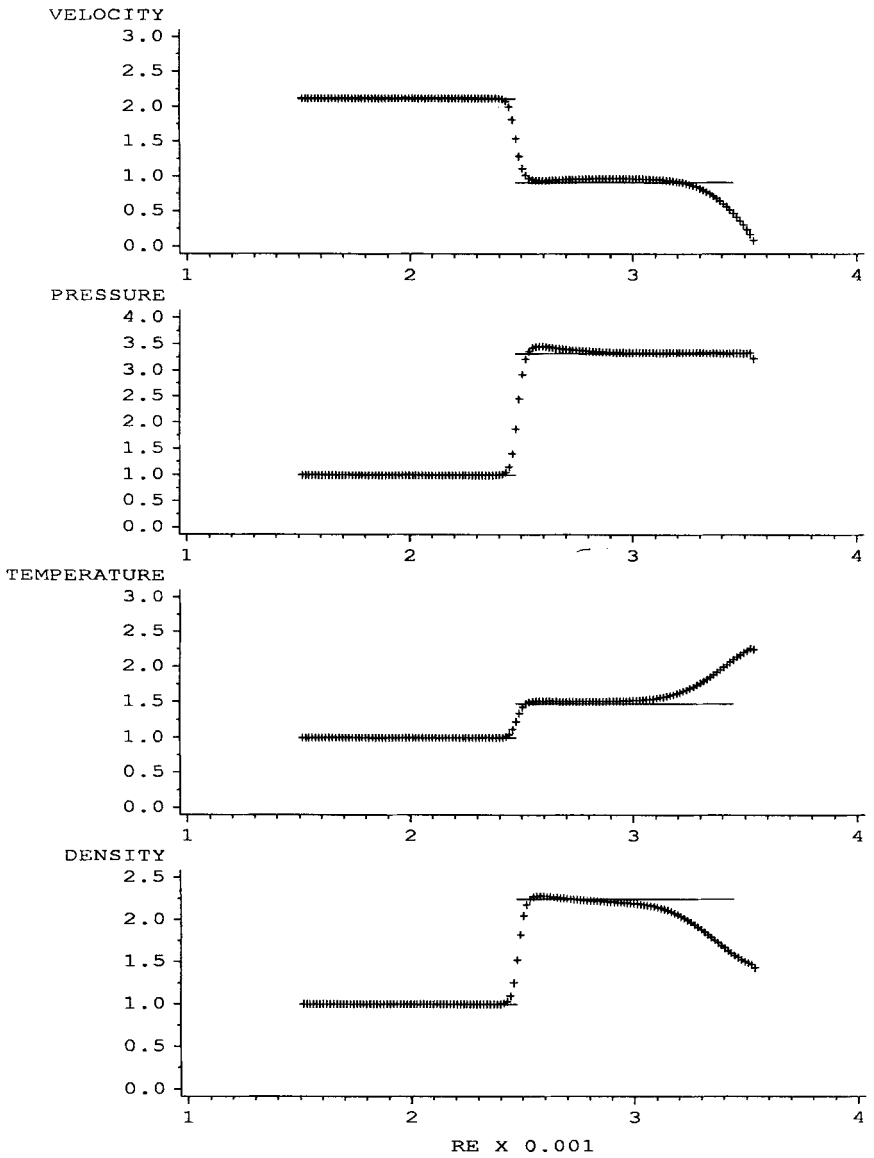

Figure 25. Flow values in a line perpendicular to the oblique shock, Mach number 2·54, shown in Figures 21–24. The thin horizontal lines indicate the value of the inviscid variables across an oblique shock of the same angle

Figure 25. The shock angle was measured as 43°. It can be seen that the computation is very close to the inviscid values for this deflection angle near the shock.

COMPUTATIONAL RESOURCES

The algorithm requires approximately 380 CPU seconds to update the example problem for one time step on a PRIME 9955 minicomputer. Approximately 5000 time steps are required for the starting shock system shown to travel across the problem domain. The large amount of computational time required means that the problem is run in background on a PRIME 9955 computer that is normally used for other purposes, and each solution requires about 4 weeks of calender time.

CONCLUSIONS

The algorithm described gives satisfactory simulations of viscous perfect gas flows at Mach numbers ranging from low supersonic to hypersonic values. The algorithm has the potential to be developed to incorporate real gas effects created by dissociation and recombination of molecules in high enthalpy flows, and further work will proceed in this direction.

ACKNOWLEDGEMENTS

The author gratefully aknowledges the encouragement and constructive criticism received from Dr. N. R. Mudford and Dr. S. L. Gai during the development of this algorithm.

REFERENCES

1. J. P. Boris and D. L. Book, 'Flux-corrected transport, I. SHASTA, a fluid transport algorithm that works', *J. Comput. Phys.*, **11**, 38–69 (1973).
2. R. Löhner, K. Morgan, J. Peraire and M. Vahdati, 'Finite element flux-corrected transport (FEM-FCT) for the Euler and Navier–Stokes equations', *Int. j. numer. methods fluids*, **7**, 1093–1110 (1987).
3. S. Chakravarthy and S Osher, 'A new class of high accuracy TVD schemes for hyperbolic conservation laws', *AIAA Paper 85-0363*, 1985.
4. H. C. Yee, R. F. Warming and A. Harten, 'Implicit total-variation diminishing (TVD) schemes for steady state calculations', *J. Comput. Phys.* **57**, 327–360 (1985).
5. W. Schmidt and A. Jameson 'Euler solvers as an analysis tool for aircraft aerodynamics', in W. G. Habashi (ed.), *Advances in Computational Transonics*, Pineridge, Swansea, 1985, pp. 371–404.
6. P. J. Roache, *Computational Fluid Dynamics*, Hermosa, Albuquerque, NM, 1976, pp. 279–282.
7. N. R. Mudford, 'Supersonic flow with fully specified properties entering a stagnant region with fully specified properties', private communication, 1989.
8. H. W. Liepmann and A. Roshko, *Elements of Gasdynamics*, Wiley, New York, 1957.